Characterization and Modeling of the Nonfaradaic Response of Ultrahigh Surface Area Carbon Fibers by Electrochemical Flow Injection Analysis

Albert J. Gotch,*,† Richard S. Kelly,‡ and Theodore Kuwana§

Department of Chemistry, Mount Union College, Alliance, Ohio 44601, Department of Chemistry, East Stroudsburg University, East Stroudsburg, Pennsylvania 18301, and Department of Chemistry, University of Kansas, Lawrence, Kansas 66045

Received: August 23, 2002; In Final Form: November 21, 2002

The ion partitioning properties of ultrahigh surface area carbon fibers (UHSACF's) have been studied using electrochemical flow injection analysis. Previous work has shown ion partitioning depends on the extent of fracture of the fiber and the charge and size of the analyte ion. We now show the polarizability of the partitioning species also plays an important role by comparing the response of electrochemically fractured fibers to monovalent inorganic cations, divalant inorganic cations, and a series of quaternary ammonium salts. Highly fractured fibers with capacitances >4000 μF/cm^2 show a reduced selectivity but an order of magnitude enhanced sensitivity to positively charged ions. This is consistent with increased surface area and increased pore size as a result of the fracture process. Previously, a simultaneous faradaic and nonfaradaic response from $K_3Fe(CN)_6$ at a UHSACF was reported. Here we apply a simple Gaussian model that provides a qualitative basis for understanding the ion flow into and out of fractured carbon fibers.

Introduction

Carbon fiber has been used for many years as a lightweight, high tensile strength material suitable for such varied applications as sporting equipment to military helicopter rotors.[1] Treated carbon fiber materials have been the object of investigations studying their use in water purification,[2−4] rechargeable batteries,[5−7] supercapacitors,[8,9] chemical sensors,[10−13] and novel electrodes.[14−16] Many of these applications use a thermal and/or chemical treatment to enhance the properties of the fibers, e.g., tensile strength and conductivity. Although all of the above applications have benefited from the unique properties of carbon fibers, further increases in efficiency may be attained by increasing the surface area of the substrate while the integrity of the carbon fiber is maintained.

In this regard, an alternative electrochemical method of treatment has been developed by Sherwood[17] and Kuwana.[18] This method consists of the anodic oxidation of the carbon fiber leading to a greater than 1000-fold increase in its capacitance. This increased capacitance is due to increased surface area, as demonstrated by concurrent increases in electron-transfer capacity[19,20] and morphological changes observed in microscopic images.[21] Related investigations have shown the presence of acidic functional groups,[17,22] affecting the chemical selectivity[19] and sensitivity[23] of these fibers for faradaic electrochemical processes.

Cyclic voltammetric (CV) studies of catechols at UHSACF electrodes[19,20] have shown that positive ions are preferentially partitioned into fractured carbon fibers under neutral to acidic conditions. Computer modeling of the faradaic current response indicates these electrodes behave like thin-layer electrochemical cells where the internal thin-layer volume depends on ion charge and pH.[20] Additional measurements of the faradaic and nonfaradaic response of these electrodes have further elucidated a size dependence associated with the cationic partitioning under "low fracture" (750−1500 μF/cm^2) conditions.[21]

UHSACF's may yield greatly increased sensitivity as biochemical sensors. Recently, this potential has been demonstrated by Pingarrón et al.[23] where the detection limit for chloramphenicol in milk was found to be 50 nM at a fractured carbon fiber electrode. This represents a 100x increase in the sensitivity compared to a Ni modified carbon electrode.

We have undertaken a series of studies to understand the fundamental selectivity and sensitivity enhancements that occur at these electrodes. The present study specifically focuses on the nonfaradaic cation partitioning properties of this novel ultrahigh surface area material. Electrochemical flow injection analysis (EC-FIA) was chosen because of its relative speed and high sensitivity. Well-defined current responses in the nano- to picoampere range are observed as ions carry charge in and out of the fiber in the partitioning process. We also show that a simple Gaussian model can qualitatively account for the observed ion partitioning responses.

Experimental Section

A single strand of DuPont E-120 carbon fiber of nominal 10 μm diameter was isolated from a small bundle of fibers, mounted on a 14 gauge copper wire using colloidal silver epoxy, and then placed in a freshly prepared 0.1 M, pH 2.2, sodium phosphate buffer solution. A series of ten CV scans between −100 and +400 mV vs saturated Ag/AgCl were made using an Omni 90 potentiostat (Cypress Systems, Lawrence, KS) and recorded with an Omnigraphic 2000 $X-Y$ recorder (Houston Instruments, Austin, TX). From the tenth or eleventh CV scan, the nonfaradaic current of the fiber was measured at +80 mV and the fiber capacitance was calculated as described previ-

* Corresponding author. E-mail: gotchaj@muc.edu. Phone: 330-823-3680.
† Mount Union College.
‡ East Stroudsburg University.
§ University of Kansas.

10.1021/jp026822v CCC: $25.00
Published on Web 01/07/2003

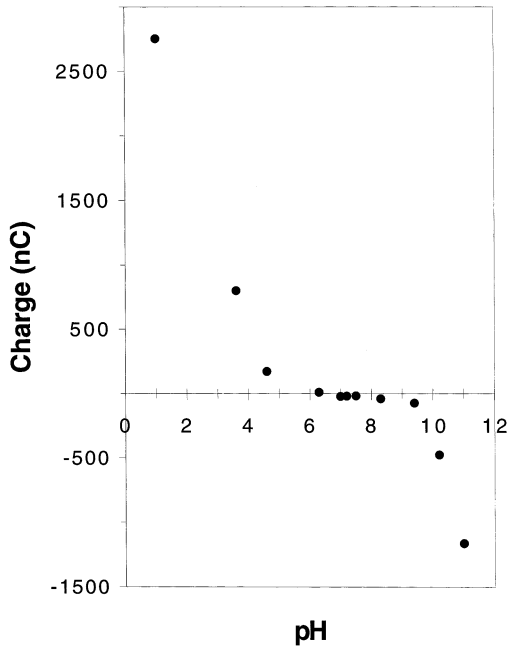

Figure 1. Nonfaradaic charge as a function of pH recorded for a single fractured carbon fiber. Fracture level 1060 μF/cm^2; mobile phase 1 mM KCH_3COO, pH 5.6; 1 mm cell, 150 mL sample loop, 0.2 mL/min flow rate. Injected samples are 1 mM KCH_3COO and pH adjusted with glacial acetic acid or KOH.

ously.[19] Prior to fracture the fiber capacitance was nominally 1−3 μF/cm^2. The fiber was then subjected to a +2.5 V constant potential to achieve the desired level of fracture. Typically, 8−40 s was required to produce final fractures in the range of 1000−6000 μF/cm^2. The fractured carbon fiber was then transferred to an in-house designed flow-cell[24] and mounted between two copper leads across a 1 mm diameter opening using colloidal silver epoxy. The fiber was equilibrated overnight with the desired background mobile phase at a very slow flow rate (ca. 0.05 mL/min) using a peristaltic pump (Alitea S1-MINI) and PEEK tubing. The background solution for unbuffered systems was usually 25 mM KNO_3 and for buffered systems 10 mM KCH_3COO at pH 5. The potential of the working electrode was adjusted so the observed background current was at or near zero in the presence of carrier solution. This generally resulted in an applied potential between 0 and ±100 mV.

EC-FIA was accomplished at a flow rate of 0.2 mL/min by injecting the desired analyte with a 100 or 150μL sample loop via a 6-way Rheodyne valve. In all experiments, the Omni 90 potentiostat was used to measure the current as a function of time on a strip chart recorder (Kipp & Zonen Model BD41, Bohemia, NY). The recorder traces were scanned into a PC, then digitized, and analyzed using UN-SCAN-IT software (Silk Software, Ogden, UT). Each experimental data point reported below represents the average of three injections with adjustment made for differences in sample loop size.

Solutions were prepared with ultrahigh purity (UHP) water from a Nanopure water system (Barnstead/Thermolyne Corp., Dubuque, IA). Analyte solutions were prepared at 25 mM of the nitrate salt for the inorganic metal cations and 25 mM of the chloride salt for the organic quaternary ammonium cations. All chemicals were reagent grade and were used as received.

Results and Discussion

Ion Partitioning. Figure 1 shows a typical response of a single fractured carbon fiber to changes in pH. As the pH of the injected sample was varied to more acidic values, larger and larger cathodic currents were measured. This is consistent with the flow of protons into the fractured carbon fiber purely on the basis of the concentration gradient.[21] Likewise, as the pH was adjusted to more basic values an anodic current was observed due to protons now moving out from the carbon fiber due to a reversal in the proton concentration gradient. Previous studies[17,22] have shown the surface of oxidized carbon materials, and specifically carbon fiber materials contain carboxylic acid and phenolic groups. The dramatic increases in nonfaradaic charge observed below pH 4 and above pH 9 are indicative of the active participation of these groups in the ion-exchange process at these pH values. The pK_a's of benzoic acid and phenol are 4.19 and 9.96, respectively, and for *o*-hydroxybenzoic acid 2.97 and 13.40.[25] Thus our data are consistent with the presence of these functional groups on the surface of the anodized carbon fiber.

One potential contribution to the observed signal is from a change in the capacitance of the fiber as the ionic strength varies. In a capacitance study vs pH done on sheets of single-wall carbon nanotubes some variation of the capacitance was observed at very acidic (60% increase) or basic conditions (20% increase).[26] These variations are much smaller than our observed increases in nonfaradaic current and are on the order of magnitude expected for changes in double-layer capacitance.[27] In the present work the nonfaradaic current response with pH has been observed over a range of background mobile phases and concentrations including 1 and 10 mM $LiNO_3$, 1, 10, and 25 mM KNO_3, and 1 and 10 mM KCH_3COO. This further indicates the pH response originates from the inherent properties of the anodized carbon fiber.

To ensure a constant pH in the remainder of the experiments presented here, mobile phase solutions were prepared from 10 mM KCH_3COO adjusted to a pH of 4.8 with glacial acetic acid. The sample solutions were 25 mM in the ion of interest made up in stock 10 mM KCH_3COO, pH 4.8. The pH of both the mobile phase and analyte solutions were verified prior to or during all experiments and did not vary more than 0.2 pH units between them. Thus, at the buffered pH the observed signal is fully attributed to the analyte ion and not pH differences between the mobile phase and the analyte solution.

Results for the monovalent group 1 cations are presented in Figure 2 with observed cathodic charge plotted as a function of ionic mobility. As the ionic mobility increases, more ion partitioning is observed. This behavior is expected because FIA is a nonequilibrium technique.[28] The injected sample has a contact time of approximately 50 s with the fiber, as determined from faradaic measurements at our flow rates.[21] The microporous internal structure of the fractured fiber provides a range of sites between the surface and the interior that can contribute to ion partitioning. At lower fracture levels access to these sites in the deep interior is limited. At higher fracture levels analyte ions have greater access to these sites. Thus, the nonfaradaic response increases as fracture level increases.

Further support of this interpretation is found in three other lines of physical evidence. (i) There is no detectable response observed when unfractured fibers are used in the cell. (ii) Fast ion bombardment images previously obtained[21] indicate the pore structure of the fiber enlarges due to the fracture process. (iii) The calculated exposed surface area of a fiber in a 1 mm cell of nominal 10 μm diameter is $2\pi rh = 31\,416\ \mu m^2$. If the entire *external surface* were covered by Na^+, assuming a hydrated ionic radius of 450 pm,[29] this would correspond to 2.47×10^{10} Na^+ ions on the surface or a charge of 3.96 nC. From Figure 2

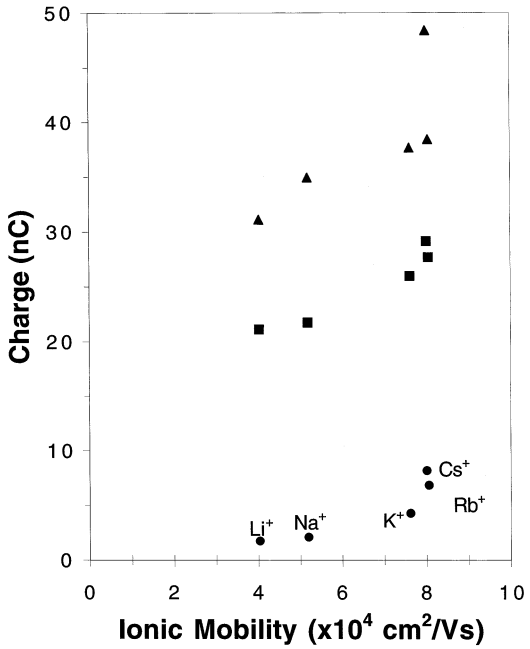

Figure 2. Nonfaradaic charge measured at several fracture levels as a function of ionic mobility. Mobile phase 10 mM KCH_3COO buffered to pH 4.9; flow rate 0.2 mL/min. Injected samples are all 25 mM of nitrate salt prepared in buffered mobile phase. Key: (●) 2377 μF/cm^2; (■) 4140 μF/cm^2; (◆) 6406 μF/cm^2.

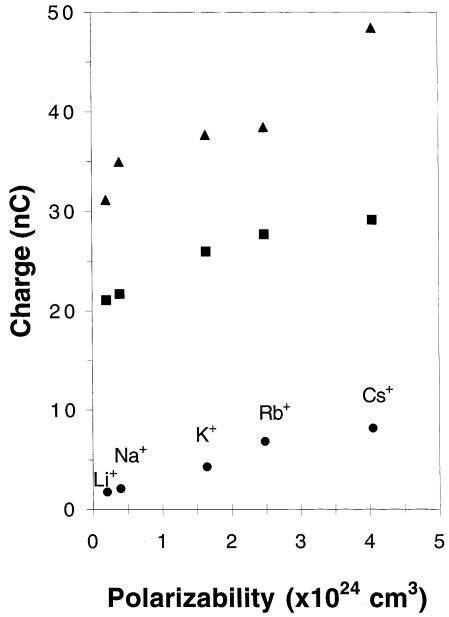

Figure 3. Monovalent cation response at a single fractured carbon fiber plotted vs core electron polarizability. See text for details. Experimental conditions identical to Figure 2. Key: (●) 2377 μF/cm^2; (■) 4140 μF/cm^2; (◆) 6406 μF/cm^2.

one can readily verify that 35 nC of charge are exchanged when Na^+ is the counterion in the high fracture fiber. The total charge observed is greater than that generated if there were 100% surface coverage of Na^+ ions. Thus, *internal charge sites* must be involved in ion partitioning, even at the lowest level of fracture.

Figure 2 also shows a clustering of the observed nonfaradaic charge with K^+, Rb^+, and Cs^+. This is a result of the similar values of ionic mobility for the three ions. However, the *charge density* of these ions decreases significantly going from K^+ to Rb^+ to Cs^+. As the charge density decreases, the polarizability of these ions increases. This factor appears to be playing a role in the partitioning process. Plots of nonfaradaic current response vs charge density are nonlinear and show an increase in the current as the charge density of the cation decreases. To understand the fundamental basis of the variations in the observed current response, we propose that the interaction potential between the analyte and the fractured carbon fiber is the sum of ion−ion and ion-induced dipole terms. Although this is an oversimplification, it does provide a valuable guide to understanding the observed ion partitioning behavior. The possible contribution of other factors such as entropy of hydration and adsorption kinetics are addressed later.

It is well established that polarizability plays an important role in ion-exchange phenomena.[29−31] However, it is the balance of primarily three factors (charge, size, and polarizability) that determine the extent of ion partitioning. In fractured fibers, ionic charge and hydrated radius are the dominant factors. Polarizability effects would be expected to play a role with large monovalent cations, like Rb^+ and Cs^+ and organic cations, e.g., tetraalkylammonium salts, where charge density is reduced and polarizability is increased, but not in divalent or trivalent metal cations. Figure 3 shows a plot where the *x*-axis is changed from ionic mobility to polarizability of the corresponding noble gases.[25] Because each monovalent cation has an electron configuration of $(n-1)s^2(n-1)p^6ns^0$, the remaining core electrons should be effectively modeled as the corresponding noble gas. Remarkably, the plot of nonfaradaic current vs polarizability is linear.

Additional support for a polarizability effect is seen with the injection of quaternary ammonium salt samples, the results of which are shown in Figure 4. The nonfaradaic currents observed for the quaternary ammonium salts show the opposite of the expected trend when plotted vs ionic mobility in Figure 4A. Instead of a decreasing response with increasing size (hydrated radius) and decreasing mobility as observed with the mono- and divalent nitrate salts (see below), an increasing response with increasing size was obtained. As already noted, charge and size are important factors in the ion partitioning phenomenon. Because the ionic sizes of the quaternary ammonium cations are significantly larger than the monovalent metal cations, their charge density is much smaller, leading to a substantial increase in polarizability.

Figure 4B shows the fiber response plotted as a function of the polarizability of the corresponding quaternary ammonium salt. Molecular polarizability is usually measured in the gas phase and was not directly available for the quaternary ammonium salts used in the current investigation. However, this property was readily calculated for each ion using Chem3D.[32] An initial optimum geometry was first obtained using MM2 molecular mechanics, and then the molecular polarizability was calculated using the semiempirical MOPAC method with MNDO, AM1, and PM3 parametrization. For comparison, the dielectric continuum model of Lorenz and Lorentz[33] was also used to calculate the electronic polarizabilities. In this case solution data of the quaternary ammonium hydroxy salts from Aldrich[34] were used. The small contribution of the water solvent to the polarizability of the solution was subtracted to arrive at the final continuum model polarizability values. The best agreement of ±8% between the continuum and molecular models was found for the AM1 method. The continuum model values of the calculated polarizabilities gave the best linear fit,[35] which were used for the plot shown in Figure 4B.

A reasonable interpretation can be made from the point of view of intermolecular forces. In this case the major driving force for the observed behavior is most likely the ion−ion

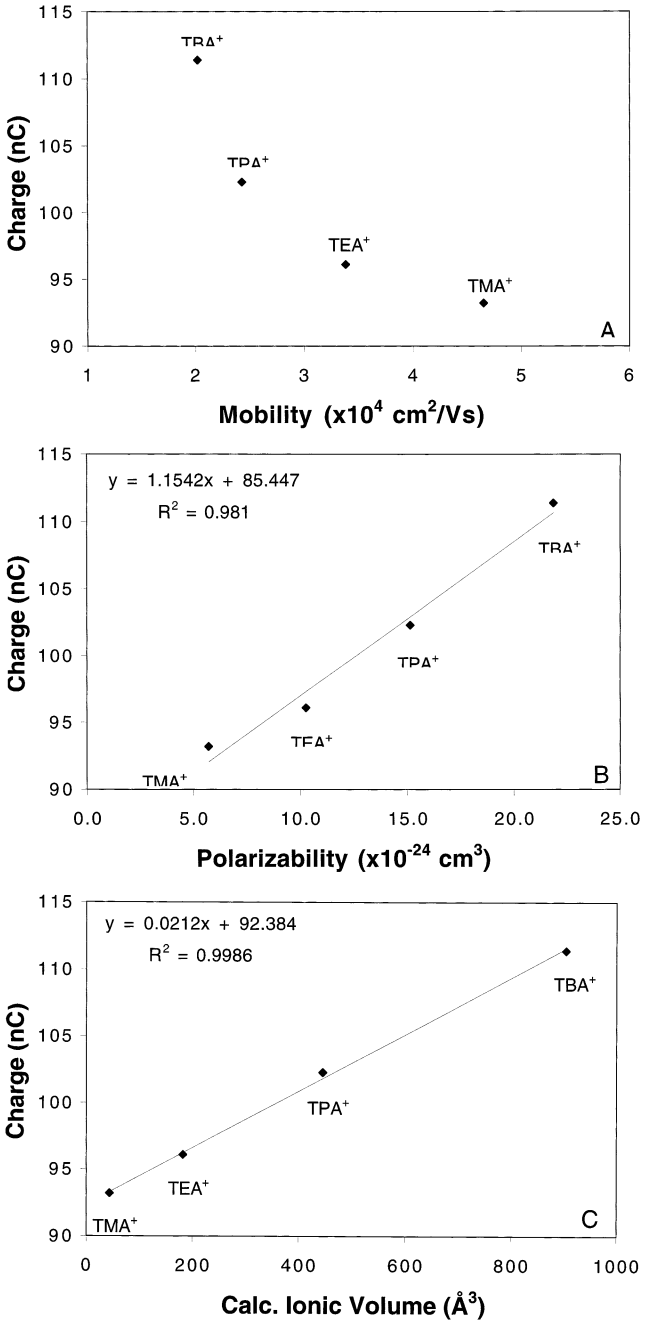

Figure 4. Monovalent quaternary ammonium cation response as a function of (A) ionic mobility, (B) continuum model polarizability, and (C) calculated volume. Fracture level 3662 μF/cm^2; mobile phase 10 mM KCH_3COO, buffered to pH 4.8; flow rate 0.2 mL/min. Injected samples are all 25 mM of chloride salt prepared in buffered mobile phase. TMA^+ = tetramethylammonium ion, TEA^+ = tetraethylammonium ion, TPA^+ = tetrapropylammonium ion, TBA^+ = tetrabutylammonium ion.

interaction. The ion-induced dipole interaction, whose magnitude is proportional to the polarizability, plays an important but secondary role. In a simple pairwise model,[33] calculations of the ion−ion interaction vs the ion-induced dipole interaction for an analyte with a 2+ charge with a fixed surface charge of 1− indicate the ion−ion interaction accounts for nearly all of the total expected interaction energy. On the other hand, the ion-induced dipole interaction becomes a larger percentage of the total interaction energy for low charge density monovalent cations. The quantitative results of these calculations are highly

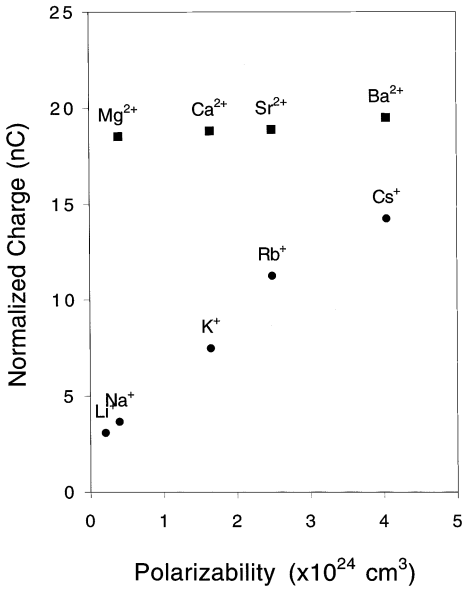

Figure 5. Comparison of mono- and divalent cation data taken at the same single fractured carbon fiber. Fracture level ca. 4100 μF/cm^2, mobile phase 10 mM KCH_3COO, buffered to pH 4.8; flow rate 0.2 mL/min. Injected samples are all 25 mM of nitrate salt.

dependent upon the ionic radii values used; however the stated general trend still holds.

Analysis of data obtained for divalent metal cations revealed that the polarization effect observed for monovalent cations was not present for divalent ions. This can be explained by the higher charge density of the divalent cations, with the Coulombic energy between the cation and the fixed charge site being twice as strong and dominant. In addition, at lower fracture levels, the sensitivity toward divalent cations was found to increase compared to fibers fractured to a higher level. This behavior has been observed in other systems[21] where a size exclusion effect was clearly seen at low fracture levels of ca. 1200 μF/cm^2. Thus the smaller pore size of the lower fractured fiber favors the ion with the greater mobility to participate in the ion partitioning process. In contrast, the current study was done at very high fracture levels, which suggests a higher porosity and a larger pore size in these carbon fibers. Figure 5 shows a comparison between mono- and divalent cations at the same high fracture level of 4100 μF/cm^2. The previous size selectivity for divalent metal cations is essentially lost whereas the general cationic selectivity is retained.

The quaternary ammonium salts may be viewed as representative of molecules that exhibit high hydrophobicity. There remains widespread use of the concept of hydrophobicity in chromatography applications,[36,37] protein stability studies,[38] QSAR relationships,[39,40] and pharmakinetics[41] whereas a clear quantitative theory is just emerging.[33,42] Fundamentally, hydrophobicity is a direct result of the positive ΔG_{solv} associated with the mixing of a substance with water. In this regard many investigators have correlated hydrophobicity with log K_{ow}.[36−38] However, theoretical studies can readily separate the enthalpic and entropic contributions to hydrophobicity. These studies show the largest effect is the negative change in entropy associated with cavity formation in the solvent to fit the solute molecule.[42] Thus, the excluded volume of the solute is the main contributing factor in the measure of hydrophobicity.[39−42] It is of interest then, to note the linear correlation between nonfaradaic current response and the calculated volume of the quaternary ammonium ion shown in Figure 4C.

Upon further reflection, it is not surprising that the ionic volume provides such a comprehensive fit of the data. The parameters previously discussed are all fundamentally related to the volume. Ionic mobility is inversely proportional to the size of the "atmosphere" an ion drags along as it transverses a potential field in solution. Thus, low ionic mobility results from a larger ionic volume, which in turn leads to a smaller nonfaradaic current response. The charge density of an ion is similarly related. A smaller charge density indicates a larger ion and thus a more polarizable electron cloud. If charge were the only factor, one would expect a smaller signal with decreasing charge density. However, with fixed charge sites present in the fractured UHSACF's, the observation is that the nonfaradaic current response increases with a charge density decrease. This indicates other factors are important and may dominate, as in the case of quaternary ammonium ion partitioning. Thus it is clear, three factors [charge (ion−ion), polarizability (ion−dipole), and hydrophobicity (hydration entropy)] all play a role and have varying degrees of effect depending on the size of the ion (charge density) and the fracture level of the fiber (porosity).

Modeling. FIA is a simple, yet powerful, method of analysis where steady-state conditions are not required for quick and reliable results.[28] This is because reproducibility is determined by the consistent flow of the analyte to, and response of, a detector to the analyte. Because the analyte stream is constantly flowing by the detector, if the above conditions are constant, then the response at the detector will follow the same time course for each replicate sample injection. Ruzicka and Hansen[28] have shown a sample plug takes on an essentially Gaussian profile if the condition $\tau = (D_m t/R^2) \geq 0.40$ is met; where D_m is the molecular diffusion coefficient, t is the time required to reach the detector, and R is the tube radius. For our experimental conditions $\tau = 0.38$, which is within 5% of the Gaussian profile condition. Thus, a simple Gaussian model was chosen for the analysis of our EC-FIA results.

In this simple model the observed current was assumed to be a sum of Gaussian components for each ionic species involved in the partitioning process. Because FIA involves a moving analyte stream, one species involved in partitioning will show two Gaussian waves in the course of one sample injection. One wave occurs as the analyte reaches the carbon fiber and one outgoing wave occurs as the pure mobile phase reestablishes the original equilibrium. The signal intensity at the detector at time t is assumed to be given by

$$I(t) = \sum_i A_i B_i e^{\{-(t-t_i)^2\}/\{2\sigma_i^2\}}$$

where A_i is a weighting factor, $B_i = \pm 1$ for cathodic or anodic wave respectively, t_i is the elution time, and σ_i is the normal Gaussian peak width.

Figure 6 shows the experimental trace recorded following the injection of 100 μL of UHP water into a 25 mM KNO_3 mobile phase.[21] As the water plug passes over the carbon fiber, there is a net loss of positive ions, which are present in excess at the fiber due to a Donnan type equilibrium. The original equilibrium is reestablished by the net influx of K^+ after the water plug has passed. As noted above, our experimental conditions allow the sample profile in FIA to be viewed as Gaussian to a first approximation. A simple two-component fit suffices to essentially reproduce the experimental result. One anodic component as K^+ moves out of the fiber, and one cathodic component after the water sample plug has passed and reequilibration of the fiber with the carrier concentration of 25 mM K^+ occurs.

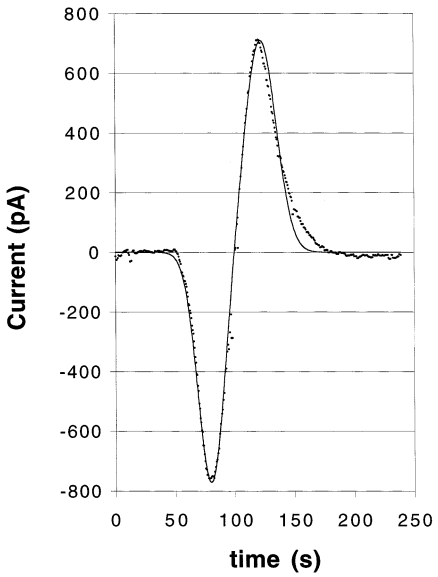

Figure 6. Comparison of two-component Gaussian fit to the experimental response of injected UHP water sample with 25 mM KNO_3 mobile phase: (●) experimental; (—) calculated. Carbon fiber fracture level ca. 1400 μF/cm^2. Fit parameters: anodic component retention time 80 s, weight 775 pA, width 11.2 s; cathodic component retention time 122 s, weight 710 pA, width, 13.2 s.

If two additional Gaussian components are used, an "exact" fit of the experimental data is obtained. The physical justification for additional components arises from the porous nature of the UHSACF's as noted above. Ion-exchange chromatograms on a silica based stationary phase have been modeled with more sophisticated methodologies,[43] which indicate a high degree of surface inhomogeniety. This is expected because of the many possible energy conformations at ion-exchange sites. In our system there are chemical differences, arenecarboxylic acid vs alkanecarboxylic acid; proximity differences, nearest neighbor sites vs second nearest neighbor sites; and structural differences, surface vs interior pore. The differences between the various carboxylic acid sites are not expected to be great on the basis of the similarities in pK_a for these groups. Certainly there will be some adjacent fixed charge sites; however, it is expected these will be a very small population of the total number of sites. Thus, we assume the differences in specific fixed charge sites are small enough to be considered as a single population modeled by a single Gaussian band. However, it is known that interior sites may have vastly different activities compared to sites in direct contact with the bulk solution on the basis of degrees of ion hydration.[44,45] For example, different models of Donnan equilibria in ion-exchange membranes used bulk dielectric values,[46] $\epsilon = 78$, or a local dielectric based on the averaged bulk + membrane dielectric,[45] $\epsilon = 6$. Because interior pore sites appear to contribute to ion partitioning into our UHSACF's, it is reasonable to expect an additional component would be needed to reflect the difference between surface sites and interior sites. In effect, the Gaussian analysis models the averaged behavior of the type(s) of site(s) rather than the true inhomogeniety that is known to be an intrinsic feature associated with ion-exchange materials.[43]

Figure 7 shows the experimental response of a UHSACF to a 100 μL injection of a solution containing 1 mM $K_3Fe(CN)_6$ and 25 mM KNO_3 with a 25 mM KNO_3 mobile phase background stream. The current scale is 10x greater than that in Figure 6 because the signal from the *faradaic* reduction of

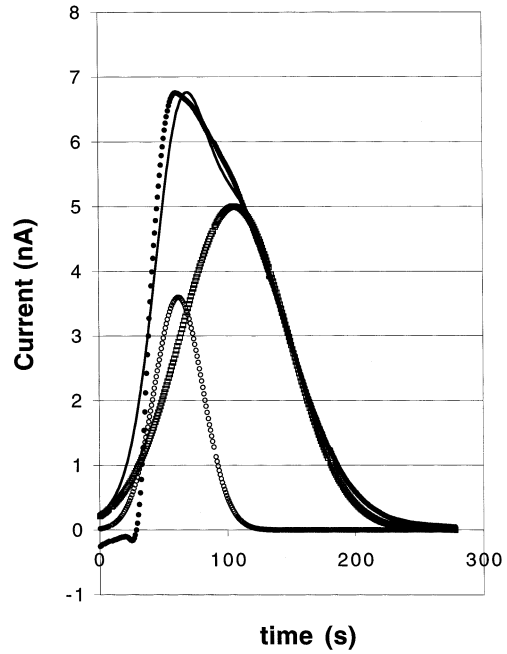

Figure 7. Gaussian deconvolution of faradaic response of analyte solution of 1 mM $K_3Fe(CN)_6$ in 25 mM KNO_3 with 25 mM KNO_3 mobile phase. Carbon fiber fractured to 3130 μF/cm^2. Key: (●) experimental; (—) calculated. Fit parameters: (○) component 1 retention time 62 s, weight 3.6 nA, width 19 s; (□) component 2 retention time 106 s, weight 5.0 nA, width, 42 s.

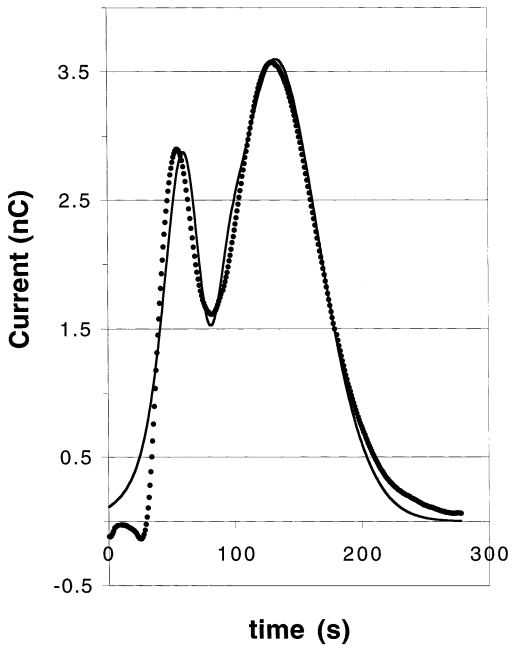

Figure 8. Experimental response and calculated fit for analyte solution injection of 1 mM $K_3Fe(CN)_6$ with 25 mM KNO_3 mobile phase. Same carbon fiber as in Figure 7. Key: (●) experimental; (—) calculated. The decreased peak intensity near 90 s is due to the K^+ concentration difference between the injected sample and mobile phase. The calculated fit is based upon a two-component fit of the faradaic response using same parameters as in Figure 7 plus two additional nonfaradaic components. Nonfaradaic fit parameters: for component 1 retention time 78 s, weight 2.2 nA, width 11 s; for component 2 retention time 89 s, weight 3.2 nA, width, 28 s.

$Fe(CN)_6^{3-}$ to $Fe(CN)_6^{4-}$ predominates when the potential at the carbon fiber is set to a less positive value. The K^+ concentration difference between the analyte and the background mobile phase is 3 mM in the above faradaic process. A control analyte sample injection of 28 mM KNO_3 with 25 mM KNO_3 mobile phase, which corresponds to a K^+ concentration difference of 3 mM, resulted in a nonfaradaic current response ca. 1−2% of the faradaic response due to $Fe(CN)_6^{3-}/Fe(CN)_6^{4-}$. Thus the nonfaradaic contribution to the total current response observed in Figure 7 can be neglected.

Also shown is the two-component Gaussian fit of the faradaic response. As noted above, these two components are interpreted as a bulk surface component and an interior pore component. This is consistent with previous modeling of faradaic processes on UHSACF's where a thin-layer and a bulk diffusive component were required to fit experimental CV data.[20]

Figure 8 shows the sum of the faradaic and nonfaradaic current response when 1 mM $K_3Fe(CN)_6$ is injected as a sample with 25 mM KNO_3 as the mobile phase. The predominant contribution to the signal is due to the reduction of $Fe(CN)_6^{3-}$. However, there is an additional component due to the significant K^+ concentration difference between the background solution of 25 mM K^+ and the injected sample which is 3 mM K^+.[47] Because the previous calculated fit of the faradaic response required two Gaussians to represent two statistically different surface regions, exterior and interior, an additional two Gaussians were used to fit the additional nonfaradaic component. The deconvoluted spectrum is not shown here; however, the ratio of the faradaic component areas from Figure 7 is 25% to 75% and the ratio of the nonfaradaic component areas from Figure 8 is 21% to 79%. This is consistent with the two-site exterior/interior model of the UHSACF's.

This Gaussian analysis using a simple physical model provides additional understanding to the current responses observed at UHSACF's in EC-FIA. A more detailed model should provide better insight into the observed transport and exchange process. Models of mass transport that explicitly solve the advection−diffusion equation in one spacial dimension lead to a Gaussian concentration profile.[48] However, these models lack inclusion of an adsorption isotherm that is central to ion partitioning and exchange phenomena. Models that include the adsorption isotherm cannot be solved analytically.[49] Numerical solutions to these models using a bi-Langmuir adsorption isotherm have proven successful in the analysis of preparative scale gas chromatography,[49] enantioselective liquid chromatography,[50] and protein elution in ion-exchange chromatography.[51]

Conclusion

We have shown polarizability effects are significant in the ion partitioning response of UHSACF's. Specifically, polarization explains the observed response of UHSACF's to large monovalent cations and provides insight into the enhanced response observed for monovalent quaternary ammonium cations. Increasing solute hydrophobicity also results in an increasing signal response at the fractured carbon fiber electrode. Generally, the response of UHSACF's increases with increasing fracture level due to the presence of more fixed charge sites and greater accessibility of the analyte to the internal pore structure of the fiber. Further work is intended to focus on the response, sensitivity, and selectivity of UHSACF's to molecules of biochemical importance that contain the quaternary ammonium motif like acetylcholine and idium salts. Here the observed enhanced sensitivity could be coupled to enhanced selectivity via faradaic activity and/or further surface modifications of UHSACF's for in vivo microsensor applications. A simple Gaussian component analysis based on a two-site physical model has clarified the nature of the electrochemical processes occurring at UHSACF's. Further insight would be

gained by modeling this system using the advection−diffusion equation with a bi-Langmuir adsorption isotherm.

Acknowledgment. We gratefully acknowledge the support provided by the University of Kansas Center for Research and the National Science Foundation (CHE-9900344). Thanks also to Mr. Prachak Inkaew for assistance in collecting the 6406 μF/cm^2 data. AJG_Dan.7.14.

References and Notes

(1) Donnet, J.-B., Wang, T. K., Peng, J. C. M., Rebouillat, S., Eds. *Carbon Fibers*, 3rd ed.; Marcel Dekker: New York, 1998.
(2) Sonoyama, N.; Sakata, T. *Environ. Sci. Technol.* **1999**, *33*, 3438.
(3) Okochi, M.; Lim, T.-K.; Nakamura, N.; Matsunaga, T. *Appl. Microbiol. Biotechnol.* **1997**, *47*, 18.
(4) Lieberman, A. I.; Pimenov, A. V.; Gorokhov, N. Y.; Shmidt, J. L.; Lieberman, L. I. Manufacture of Activated Carbon Fiber. U.S. Patent 5,-521,008, May 28, 1996.
(5) Lee, J. K.; An, K. W.; Ju, J. B.; Cho, B. W.; Cho, W. I.; Park, D.; Yun, K. S. *Carbon* **2001**, *39*, 1299.
(6) Zou, X.; Maesako, N.; Nomiyama, T.; Horie, Y.; Miyazaki, T. *Solar Energy Mater. Solar Cell*s **2000**, *62*, 1333.
(7) Suzuki, K.; Iijima, T.; Wakihara, M. *Electrochim. Acta* **1999**, *44*, 2185.
(8) Nakagawa, H.; Shudo, A.; Miura, K. *J. Electrochem. Soc.* **2000**, *147*, 38.
(9) Yamaguchi, K.; Suzuki, J.; Saito, M.; Sekine, K.; Takamura, T. *J. Power Source* **2001**, *97*, 159.
(10) de Carvalho, R. M.; de Oliveira Neto, G.; Kubota, L. T. *Anal. Lett.* **2000**, *33*, 425.
(11) Pontié, M.; Gobin, C.; Pauporté, T.; Bedioui, F.; Devynck, J. *Anal. Chim. Acta* **2000**, *411*, 175.
(12) Bedioui, F.; Trévin, S. *Biosens. Bioelectron.* **1998**, *13*, 227.
(13) Pei, J.; Yu, N.-T.; Li, X.-Y. *Anal. Chim. Acta* **1999**, *402*, 145.
(14) Bessel, C. A.; Laubernds Park, K.; Rodriguez, N. M.; Baker, R. T. K. *J. Phys. Chem. B* **2001**, *105*, 1115.
(15) Yang, W.-C.; Yu, A.-M.; Chen, H.-Y. *J. Chromatog. A* **2001**, *905*, 309.
(16) Logman, M. J.; Budygin, E. A.; Gainetdinov, R. R.; Wightman, R. M. *J. Neurosci. Methods* **2000**, *95*, 95.
(17) Xie, Y.; Sherwood, P. M. A. *Appl. Spectrosc.* **1990**, *44*, 1621 and references within.
(18) Swain, G. M.; Kuwana, T. *Anal. Chem.* **1992**, *64*, 565.
(19) Kelly, R. S.; Weiss, D. J.; Chong, S. H.; Kuwana, T. *Anal. Chem.* **1999**, *71*, 413.
(20) Weiss, D. J.; Kelly, R. S.; Cumaranatunge, M.; Kuwana, T. *Anal. Chem.* **1999**, *71*, 3712.
(21) Kelly, R. S.; Coleman, B.; Huang, T.; Inkaew, P.; Kuwana, T. *Anal. Chem.* **2002**, *74*, 6364.
(22) McCreary, R. L. In *Electroanalytical Chemistry*; Bard, A. J., Ed.; Marcel Dekker: New York, 1991; Vol. 17.
(23) Agüí, L.; Guzmán, A.; Yáñez-Sedeño, P.; Pingarrón, J. M. *Anal. Chim. Acta* **2002**, *461*, 65.
(24) Anderson, M. Ph.D. Thesis, University of Kansas, Lawrence, KS, 2000.
(25) *CRC Handbook of Chemistry and Physics*, 72nd ed.; Lide, D. R. Ed.; CRC Press: Boca Raton, FL, 1991.
(26) Barisci, J. N.; Wallace, G. G.; Baughman, R. H. *J. Electroanal. Chem.* **2000**, *488*, 92.
(27) Bard, A. J.; Faulkner, L. R.*Electrochemical Methods: Fundamentals and Applications*; Wiley & Sons: New York, 1980.
(28) Ruzicak, J.; Hansen, E. H. *Flow Injection Analysis*, 2nd ed.; Wiley & Sons: New York, 1988.
(29) Harris, D. C. *Quantitative Chemical Analysis*, 5th ed.; W. H. Freeman: New York, 1998.
(30) Kressman, T. R. E.; Kitchener, J. A. *J. Chem. Soc.* **1949**, 1208.
(31) Kunin, R. *Elements of Ion Exchange*; Reinhold Publishing Corp.: New York, 1960; p 13.
(32) *Chem 3D Pro*, version 5.0; Cambridge Soft Corp.: Cambridge, MA, 1999.
(33) Israelachvili, J. *Intermolecular and Surface Forces*, 2nd ed.; Academic Press: London, 1992.
(34) *Handbook of Fine Chemicals and Laboratory Equipment*; Aldrich: Milwaukee, WI, 2000−2001.
(35) Linear correlations for MOPAC polarizabilities; AM1, $r^2 = 0.945$; MNDO, $r^2 = 0.967$; PM3 $r^2 = 0.951$.
(36) Valkó, K.; Bevan, C.; Reynolds, D. *Anal. Chem.* **1997**, *69*, 2022.
(37) Rippel, G.; Bede, A.; Szepesy, L. *J. Chromatogr., A* **1995**, *697*, 17.
(38) Feng, Z.-P.; Zhang, C.-T. *Int. J. Biol. Macromol.* **2001**, *28*, 255.
(39) Geban, O.; Ertepinar, H.; Yurtsever, M.; Özden, S.; Gümüs, F. *Eur. J. Med. Chem.* **1999**, *34*, 753.
(40) Famini, G. R.; Loumbev, V. P.; Frykman, E. K.; Wilson, L. Y. *Quant. Struct.-Act. Relat.* **1998**, *17*, 558.
(41) Kodaka, M.; Dohta, Y.; Rekonen, P.; Okada, T.; Okuno, H. *Biophys. Chem.* **1998**, *75*, 259.
(42) Graziano, G. *J. Phys. Chem. B* **2000**, *104*, 9249.
(43) Stanley, B. J.; Krance, J.; Roy, A. *J. Chromatogr. A* **1999**, *865*, 97.
(44) Bockris, J. O'M.; Reddy, A. K. N. *Modern Electrochemistry*; Plenum: New York, 1970; Chapter 7.
(45) Mafe, S.; Ramirez, P.; Tanioka, A.; Pellicer, J. *J. Phys. Chem. B* **1997**, *101*, 1851.
(46) Hsu, J.-P.; Liu, B.-T. *J. Phys. Chem. B* **1997**, *101*, 7928.
(47) Control experiments using 3 mM KNO_3 injected into the 25 mM KNO_3 mobile phase were also done. The weighting factors obtained for the nonfaradaic contribution via this control varied with the fracture level of the fiber. These results do not affect the two-site model interpretation. See Figure 10 in ref 21.
(48) Hemond, H. F.; Fechner, E. J. *Chemical Fate and Transport in the Environment*; Academic Press: San Diego, 1994.
(49) Staerk, D. U.; Shitangkoon, A.; Wichester, E.; Vigh, G.; Felinger, A.; Guiochon, G. *J. Chromatogr. A* **1996**, *734*, 289.
(50) Fornstedt, T.; Zhong, G.; Bensetiti, Z.; Guiochon, G. *Anal. Chem.* **1996**, *68*, 2370.
(51) Gallant, S. R.; Kundu, A.; Cramer, S. M. *J. Chromatogr. A* **1995**, *702*, 125.